

SO₂ degassing at Tungurahua volcano (Ecuador) between 2007 and 2013: Transition from continuous to episodic activity



Silvana Hidalgo^{a,*}, Jean Battaglia^b, Santiago Arellano^c, Alexander Steele^a, Benjamin Bernard^a, Julie Bourquin^a, Bo Galle^c, Santiago Arrais^a, Freddy Vásconez^a

^a Instituto Geofísico – Escuela Politécnica Nacional, Ladrón de Guevara E11-253 y Andalucía, 6to piso ed. Ing. Civil, Quito, Ecuador

^b Laboratoire Magmas et Volcans, Université Blaise Pascal–CNRS–IRD, OPGC, 5, Rue Kessler, 63038 Clermont-Ferrand, France

^c Department of Earth and Space Sciences, Chalmers University of Technology, Göteborg, Sweden

ARTICLE INFO

Article history:

Received 21 July 2014

Accepted 18 March 2015

Available online 11 April 2015

Keywords:

SO₂ degassing

Tungurahua

DOAS

Open and closed system behaviour

Episodic volcanic

Activity

ABSTRACT

We present continuous SO₂ measurements performed at Tungurahua volcano with a permanent network of 4 scanning DOAS instruments between 2007 and 2013. The volcano has been erupting since September 1999, but on the contrary to the first years of eruption when the activity was quasi-continuous, the activity transitioned in late 2008 towards the occurrence of distinct eruptive phases separated by periods of quiescence. During our study period we distinguish 11 phases lasting from 17 to 527 days separated by quiescence periods of 26 to 184 days. We propose a new routine to quantify the SO₂ emissions when data from a dense DOAS monitoring network are available. This routine consists in summing all the highest validated SO₂ measurements among all stations during the 10 h of daily working-time to obtain a daily observed SO₂ mass. Since measurement time is constant at Tungurahua the “observed” amounts can be expressed in tons per 10 h and can easily be converted to a daily average flux or mass per day. Our results provide time series having an improved correlation on a long time scale with the eruptive phases and with quiescence periods. A total of 1.25 Mt (1.25×10^9 kg) of SO₂ has been released by Tungurahua during the study period, with 95% of these emissions occurring during phases of activity and only 5% during quiescence. This shows a contrast with previous volcanic behaviour when passive degassing dominated the total SO₂ emissions. SO₂ average daily mass emission rates are of 73 ± 56 t/d during quiescent periods, 735 ± 969 t/d during long-lasting phases and 1424 ± 1224 t/d during short-lasting phases. Degassing during the different eruptive phases displays variable patterns. However, two contrasting behaviours can be distinguished for the onset of eruptive phases with both sudden and progressive onsets being observed. The first is characterised by violent opening of the conduit by high energy Vulcanian explosions; and the second by a progressive, *in crescendo*, development of the activity. The first case is becoming more frequent at Tungurahua making the volcano more dangerous and less predictable.

© 2015 Elsevier B.V. All rights reserved.

1. Introduction

1.1. Gas measurements on volcanoes

Surveillance of the composition and emission rate of gases from volcanoes is very important for understanding volcanic activity, especially in conditions where degassing processes have a dominant control on eruption style (Sparks et al., 1997; Oppenheimer, 2003). Volcanoes emit different gaseous species such as H₂O, CO₂, SO₂, HCl,

HF, H₂, S₂, H₂S, CO, and SiF₄ (Symonds et al., 1994) to the atmosphere during or between eruptions, through erupting vents, fumaroles or diffused through soil.

In order to obtain the concentrations of the different volcanic species, fumaroles can be sampled and collected in different condensing systems for subsequent laboratory analysis, or measured in situ using portable electrochemical devices. This approach allows a detailed geochemical and isotopic characterisation of the gas sample, giving strong constraints on the subsurface temperature of the volcanic-hydrothermal systems and the gas source (Allard et al., 1991; Ohba et al., 2008; Rouwet et al., 2009; Vaselli et al., 2010). Nevertheless, given the high risk implied by direct sampling, routine sampling and analysis are hard to sustain in a continuous way (Symonds et al., 1994). Besides, only peripheral emissions can usually be sampled, which may show an important degree of atmospheric dilution, thus not actually representing the conditions of the magmatic system (McGonigle and Oppenheimer, 2003).

* Corresponding author.

E-mail addresses: shidalgo@igepn.edu.ec (S. Hidalgo),

J.Battaglia@opgc.univ-bpclermont.fr (J. Battaglia), santiago.arellano@chalmers.se (S. Arellano), asteele@igepn.edu.ec (A. Steele), bbarnard@igepn.edu.ec (B. Bernard), gingerchip@yahoo.com (J. Bourquin), bo.galle@chalmers.se (B. Galle), sarraais@igepn.edu.ec (S. Arrais), fvasconez@igepn.edu.ec (F. Vásconez).

Remote sensing techniques such as COSPEC (Millán, 1980; Stoiber et al., 1983) and DOAS-based instruments (Edmonds et al., 2003; Galle et al., 2003) have been useful in measuring SO₂ fluxes in active (explosive), or passive (quiescent)-degassing volcanoes. The major advantage of these instruments with respect to direct sampling lies in the possibility of making long-term, integrated and frequent measurements of SO₂ (and other species in the case of DOAS), providing temporal series that could be correlated to seismic or ground deformation data (Conde et al., 2013; Nicholson et al., 2013; Zuccarello et al., 2013). For instance, the SO₂ flux data obtained with COSPEC at Etna, Pinatubo, Mount St. Helens, as well as in other erupting volcanoes, were useful tools to forecast eruptive activity (Malinconico, 1979; Casadevall et al., 1983; Daag et al., 1994).

Since the early 2000s the DOAS portable or automated systems have gradually replaced the COSPEC. The miniature UV-DOAS systems offer a series of advantages with respect to COSPEC, given their low cost and reduced size and weight (Galle et al., 2003). The mobile equipments are therefore affordable for observatories and easily transported in order to make traverses under the volcanic plume to quantify the emission flux. Moreover, the automatic scanning DOAS stations are quite resistant to very exigent weather conditions, allowing the installation of permanent instruments in the field for continuous SO₂ flux measurement (Edmonds et al., 2003; Arellano et al., 2008; Burton et al., 2009; Salerno et al., 2009; Conde et al., 2013). As a consequence, there has been a widespread adoption of this technique by volcanological observatories, largely as part of the NOVAC network for volcanic plumes monitoring (Galle et al., 2010).

Continuous gas emission datasets allow more detailed studies of degassing processes, revealing different SO₂ emission patterns associated with diverse eruptive dynamics and conduit processes. For instance, Burton et al. (2009) support their model of magma circulation at Stromboli during the 2007 eruption using the pattern of almost continuous SO₂ measurements obtained from the FLAME network. Besides, the volume of degassed magma can be estimated by measuring the original content of sulphur (S) in magmatic inclusions and in the degassed melt (Self et al., 2004; Spilliaert et al., 2006; Shinohara, 2008; Métrich et al., 2010). Combining the volatile content in inclusions with good quality estimates of the released sulphur it is possible to obtain a better constraint of the amount of the so-called excess degassing in arc volcanoes (Shinohara, 2008).

Volcanic degassing occurs under explosive or passive emission styles and it is also common to distinguish between continuously and sporadically degassing volcanoes (Shinohara, 2008). Explosive degassing has the potential to produce columns reaching up to stratospheric altitudes. Passive degassing on the contrary can be produced without any magma extrusion. This degassing modality is also known as quiescent or non-eruptive. Passive degassing might last for long periods of time yielding important amounts of gas comparable to or larger than emissions from large explosive eruptions (Shinohara, 2008).

Andres and Kasgnoc (1998) published an inventory of volcanic sulphur emissions (up to 1997), including 49 continuously degassing volcanoes which exhibit persistent Hawaiian, Strombolian or Vulcanian activity, and 25 sporadically emitting volcanoes, which show more explosive but short-term eruptions (e.g. El Chichón, Pinatubo, Rabaul, Kilauea, Augustine). Comparing the amount of SO₂ emitted by both types of volcanoes on an annual basis, sporadically emitting volcanoes account for less than 1% of the total estimate of SO₂ emissions. This highlights the overwhelming importance of continuously degassing volcanoes.

1.2. Geological setting and eruptive activity of Tungurahua since 1999

Tungurahua volcano is located in central Ecuador, 120 km south of Quito. It is a 5023 m-high andesitic stratovolcano with a basal diameter of 16 km and a maximum relief of 3200 m. Tungurahua is built over the basement units of the Cordillera Real. Hall et al. (1999) distinguish three

different edifices, Tungurahua I, II, and III, the latter being the present volcano. The two former edifices suffered giant landslides associated with large debris avalanche deposits found in the Chambo and Patate valleys. The activity of Tungurahua III began with the Las Juntas lava flow at about 2300 years BP (Hall et al., 1999). Since 1300 AD moderate to large eruptions producing pyroclastic flows and tephra fallouts have occurred every century, in 1533, 1640, 1773, 1886, and 1918 (Le Pennec et al., 2008).

The present eruption of Tungurahua began in September 1999 and persists until the time of writing. Until May 2006 the activity was characterized mainly by gas and ash emissions of low to moderate intensity and discrete Strombolian and Vulcanian explosions. Six quiescence periods were observed between 1999 and 2004, two of them very short, lasting 8 and 9 days; and four of intermediate duration lasting 94, 54, 58 and 46 days. A long quiescence of 353 days was observed in 2005 (Fig. 2a). During the whole period intense episodes of ash emission affected the local population (e.g., late 1999, August 2001) (Le Pennec et al., 2012). In May 2006 a sustained increase in activity led to two pyroclastic-flows forming eruptions: a VEI-2 in July 2006 and a VEI-3 in August 2006 (Arellano et al., 2008; Samaniego et al., 2011; Eychenne et al., 2012). These eruptive paroxysms resulted from the relatively rapid arrival of voluminous, gas rich magma from depth to an already open-vent erupting volcano according to Samaniego et al. (2011) and Eychenne et al. (2012). A detailed description of the pyroclastic flow deposits and the eruptive sequence of the 16–18 August eruption can be found in Douillet et al. (2013a, 2013b) and Hall et al. (2013). The petrological study of the juvenile material of this eruption allowed constraining a depth of 8 to 10 km below the summit for a magmatic reservoir below Tungurahua (Samaniego et al., 2011).

Since 2007 we can roughly distinguish four eruptive periods based on the duration of eruptive phases (Fig. 2b). (1) From February 2007 until August 2008 the volcano produced a long-lasting eruptive phase (527 days), (2) Between December 2008 and May 2011, six eruptive phases of intermediate duration (37 to 98 days) took place separated by 26 to 179 days of quiescence. (3) From November 2011 until September 2012 an almost continuous activity was present being more intense at the beginning and at the end of this period. (4) Short-lasting eruptive phases with durations between 17 and 27 days, separated by quiescence periods between 41 and 58 days, occurred since December 2012 until August 2013. During these periods the eruptive activity included episodic explosions of Strombolian and Vulcanian styles, sub-continuous ash emissions and lava fountaining. Pyroclastic flows were also produced during some of these phases either fed by sustained lava fountains or triggered by Vulcanian events. Small to moderate ash emissions were common throughout periods of activity (Bernard et al., 2013).

The first SO₂ flux measurements at Tungurahua were done using a COSPEC. Fluxes of about 2500 t/d were observed at the beginning of the present eruptive period in August 1999, and up to 11,000 t/d were measured in October 1999, presumably when magma reached the surface. The first DOAS automatic scanning network installed at Tungurahua was very similar to the one installed at Montserrat (Edmonds et al., 2003) and operated from June 2004 to November 2007. This network allowed us to record the first set of continuous SO₂ measurements at the volcano and to make correlations between SO₂ fluxes and seismicity (Arellano et al., 2008).

Up to 2007 Tungurahua can be classified as a continuously degassing volcano despite the low fluxes recorded during quiescent periods. Arellano et al. (2008) distinguish between passive and explosive degassing patterns during 1999–2006, based on a threshold of explosiveness measured by seismic sensors. The inferred phases of explosive degassing were manifested superficially by lava fountains, Strombolian episodes, Vulcanian explosions and regional ash fallout. On the contrary, passive degassing corresponded to low activity phases with weaker gas emissions and occasionally a limited amount of ash. The mean SO₂ emission rates measured during 1999–2006 were about

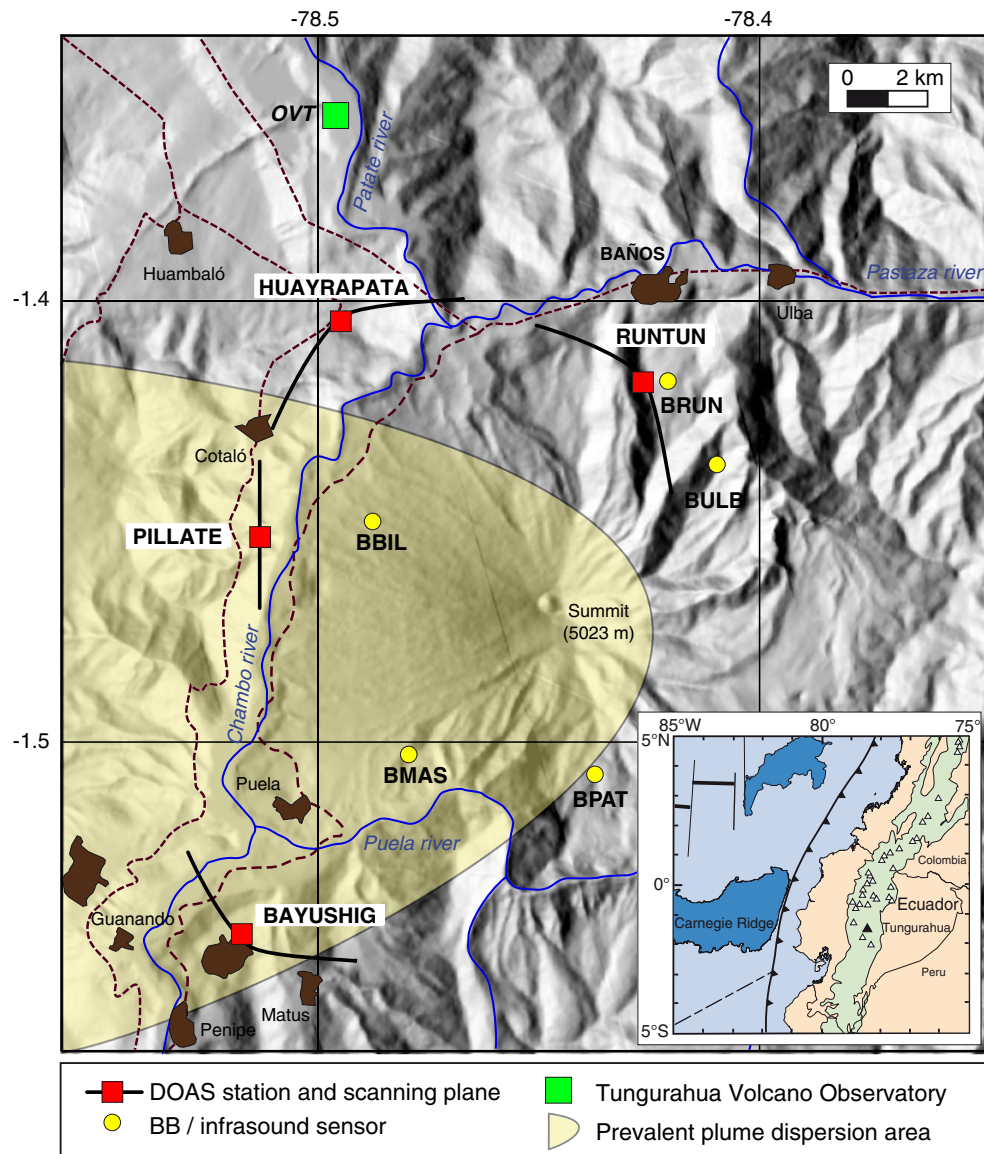


Fig. 1. SO₂, seismic broadband and infrasound monitoring networks at Tungurahua Volcano. DOAS stations are shown in red with the corresponding scanning plane (flat or conic). Broadband seismic stations and infrasound detectors are shown in yellow. The location of the Tungurahua Volcano Observatory is shown in green and a shaded area indicates the predominant direction of the plume. The main rivers and roads as well as populated areas are also shown.

2400 ± 4600 (±1σ) t/d for explosive degassing and 1400 ± 1700 (±1σ) t/d for passive degassing (Arellano et al., 2008).

In this paper we describe and analyse the degassing patterns registered by the gas flux sensors at Tungurahua since February 2007. In particular we intend to study the change in eruptive style from quasi-continuous degassing, as it was observed during the first years of the eruption, to an alternation of periods of quiescence and low-to-high intensity explosive activity phases.

2. DOAS measurements and monitoring network

2.1. DOAS technique

The principle to quantify volcanic gas fluxes using scanning instruments is a straightforward application of mass conservation in a volume enclosing the volcanic source. The scanning surfaces of the instruments surrounding a volcano define a volume (bounded from below by the ground and considered limited from above by the highest measurable altitude of the plumes) within which the main source of emission is

the volcano. Thus, if no other important sources (e.g., anthropogenic sources, chemical reactions) are present and if loss mechanisms (e.g., ground deposition, chemical reactions, adsorption in tephra, solution in aerosols, atmospheric dilution) can be neglected, the source strength is equivalent to the integral of the normal component of the flux density across the scanned surfaces. This integral is obtained by summing the column densities of the gas of interest along the transversal direction of transport, which are obtained by the spectroscopic method known as DOAS (Platt and Stutz, 2008), and multiplying the result by the normal component of the transport speed, assumed to be equal to the wind speed at a representative altitude of the plume.

2.2. DOAS network at Tungurahua

The DOAS monitoring network at Tungurahua is composed of 4 NOVAC version I instruments (Galle et al., 2010). The stations are located at Huayrapata, 9.1 km Northwest of the volcano summit, Pillate, 8 km West, Bayushig, 11.9 km Southwest and Runtún, 5 km North (Fig. 1). Huayrapata and Bayushig were installed on March 17 and 30, 2007,

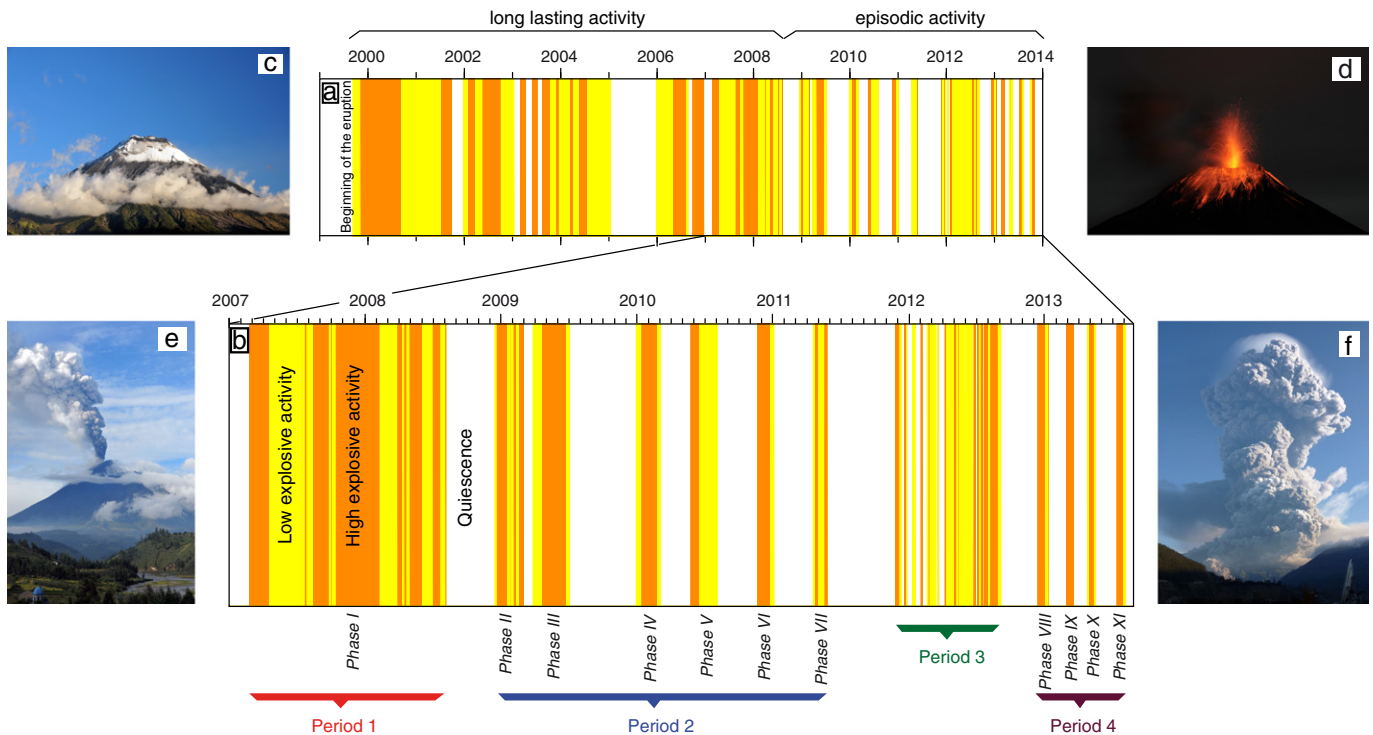


Fig. 2. Periods and phases of activity distinguished at Tungurahua volcano. a) September 1999 to August 2013. b) January 2007 to August 2013. White background indicates periods of quiescence. Yellow and orange represent low (LEA) and high (HEA) explosive activity respectively. c) Tungurahua during quiescence phases. d) and e) Typical lava fountaining (500 m above crater level) and ash venting during low explosive activity (2 km above crater level). e) Vulcanian eruption at Tungurahua, eruptive column reaches 8.8 km above crater level.

on the same sites as the previous stations described by Arellano et al. (2008). Pillate was installed on November 15, 2007, on a site located in the direction of the prevailing winds. Runtún was installed on February 23, 2011, to cover the occasional winds blowing to the North from November to December. These sites give us an almost complete coverage for plumes heading towards S to NE (clockwise), leaving only a coverage gap for infrequent plumes transported to the E-SE. Each station works during daylight from 07:00 to 17:00 (local time), all year long since sunrise and sunset times are almost constant at the latitude of the volcano. Each individual scan takes between 3 and 14 min, depending on the light intensity, yielding for each instrument a total of 50 to 140 scans per day. The collected data are transmitted in real time by radio link to the Tungurahua Volcano Observatory (Fig. 1), where they are evaluated by the NOVAC software (Johansson et al., 2009) and post-processed daily by the observatory staff, to account for the best available wind information. Since the installation of the DOAS network the instruments have been operational for about 86% of the time for Bayushig, 85% for Pillate, and 78% for Huayrapata and Runtún.

2.3. Data processing

The NOVAC software performs an automatic preliminary SO₂ flux estimation during acquisition using default or operator pre-set wind parameters (wind speed and wind direction) and plume height (Galle et al., 2010). For Tungurahua, we use the forecasted ECMWF data (<http://www.ecmwf.int>) as the default wind parameters with a time resolution of 6 h and interpolated to the coordinates of the volcanic summit. For the plume height we assume that emissions are confined to the summit altitude of the volcano. In order to incorporate real wind conditions and plume height, which constitute an important source of error (Burton et al., 2009; Johansson et al., 2009; Salerno et al., 2009), data are post-processed on a daily basis. To post-process the data, we determine the wind speed, the wind direction and the plume height for the different time periods when triangulation between

data from at least two stations is possible (Arellano et al., 2008). The only input required for this processing is the wind speed, which is taken from the VAAC (Volcanic Ash Advisory Centre) when available, or from the ECMFW (analysed data). This file is imported into the NOVAC software and SO₂ fluxes are calculated using the wind parameters and plume height obtained by triangulation. This geometrical strategy is not always possible when SO₂ emissions are very low or not continuous during the day, or when clouds affect the measurement conditions at one or more of the stations. In such a case we use a standard plume height at the altitude of the volcano summit assuming the plume is drifting at the summit's altitude (5 023 m asl) and wind velocity and direction from the ECMWF (analysed data for the corresponding day) for the flux calculation.

After post-processing a list is generated including the time of all valid scans taken during the day and their corresponding SO₂ fluxes, as well as ancillary information (plume speed, direction, height, number of spectra per scan, etc.). Valid scans are those in which SO₂ is measured (good spectroscopic fitting, see Galle et al., 2010 for details) and plume completeness is higher than 0.5 (an empirical measure of how well the scan captures the entire plume, equal to 1 when spectra from the low scan angles do not include signatures of the volcanic gas, Johansson, 2009). For some days the programme validates only few or no scans. This can be related to several factors: plume drifting in a direction not covered by the network (SE for Tungurahua), adverse weather conditions (heavy rain or dense fog), very low SO₂ emissions or very large amounts of ash or aerosols emitted from the volcano. The number of daily validated measurements varies, however, strongly and empirically we note that this number is usually much higher during periods of activity than during quiescence. This suggests that the low values or absence of SO₂ during quiescence periods is the major source of scan rejection.

It is noteworthy that there is an important error in the gas flux measurements performed by DOAS instruments. This error is estimated to be about 26% under good measuring conditions and about 54% under fair conditions (Galle et al., 2010; Kern et al., 2010).

3. Evaluation of daily SO₂ emissions

The conventional way to process SO₂ flux data, while using single or a few daily COSPEC or Mobile DOAS measurements is to average the obtained fluxes and extrapolate them as a daily flux, implicitly assuming that those measurements are representative of the whole day SO₂ emission (i.e. daily SO₂ mass). This practice is specially used for monitoring purposes in order to follow the evolution of degassing and provide scenarios of eruptive activity on a daily basis. This extrapolation is somehow justified by the reduced number of measurements and by the fact that when performing COSPEC or Mobile-DOAS the operator is able to constrain the width, height and direction of the plume, reducing therefore the uncertainties in the corresponding calculated flux. However, bad weather conditions or the presence of considerable amounts of ash might prevent obtaining reliable estimates. Moreover, activity may be highly variable during a single day, displaying sporadic or continuous degassing, and even in this last case, SO₂ fluxes can strongly vary during the length of a same day. Automated DOAS stations have the advantage of producing a high number of daily measurements and giving insights into the temporal evolution of degassing, with the condition that the plume axis lays within a certain range of directions above the station. The use of multiple monitoring stations allows us to cover different wind directions in which the plume might be dispersed. Averaging variable amounts of measurements to obtain extrapolated SO₂ daily emission may sometimes be an oversimplified approach, especially when a dense network is present. Therefore, in order to obtain more accurate daily estimations of the SO₂ emission, we developed a method that takes into account all measurements taken from the 4 stations to obtain a daily observed SO₂ mass.

3.1. Extrapolated SO₂ daily emissions

An advantage of using the NOVAC-DOAS stations is the possibility of having numerous SO₂ measurements per day. At the Tungurahua Volcano Observatory, the standard way to process these data is to calculate the average of all valid measurements individually for each station and then report the highest average daily value obtained. This assumes that the highest average represents the best estimate of the true real flux when the plume direction does not vary much across the day. This approach presents, however, some inconveniences. First, the instruments work only during daylight hours (10 h at Tungurahua's latitude). Consequently, when extrapolating the measured average, it is assumed that the daylight SO₂ emission rate is also representative of the night time period. Second, the number of valid measurements is variable depending on the factors mentioned above, especially during phases of low or no eruptive activity when instruments record only a few valid measurements (<10) and which in some cases may reach relatively high SO₂ flux values (> 1000 t/d for Tungurahua). Extrapolating these few measurements may thus result in an overestimation of the actual daily SO₂ emission. Besides, while prevalent wind direction at Tungurahua is to the West, variations can occur during the day and accordingly higher recorded values from other stations might be ignored because only the station with the highest daily average is taken into account.

To examine the influence of the data selection in the calculation of extrapolated SO₂ daily emissions, we tested different thresholds for the plume completeness parameter: 0.5, 0.8 and 0.9 (Fig. 3). Using a threshold of 0.8 slightly reduces the number of validated measurements and provides comparable SO₂ emissions to those obtained by using a plume completeness threshold of 0.5 (Fig. 3a). On the contrary, the 0.9 threshold reduces drastically the number of valid measurements (Fig. 3b). In particular, during quiescence phases the number of validated measurements is often very low or even null and therefore the extrapolated daily emissions may be significantly reduced or can be zero despite the fact that SO₂ has been partially observed by the instruments.

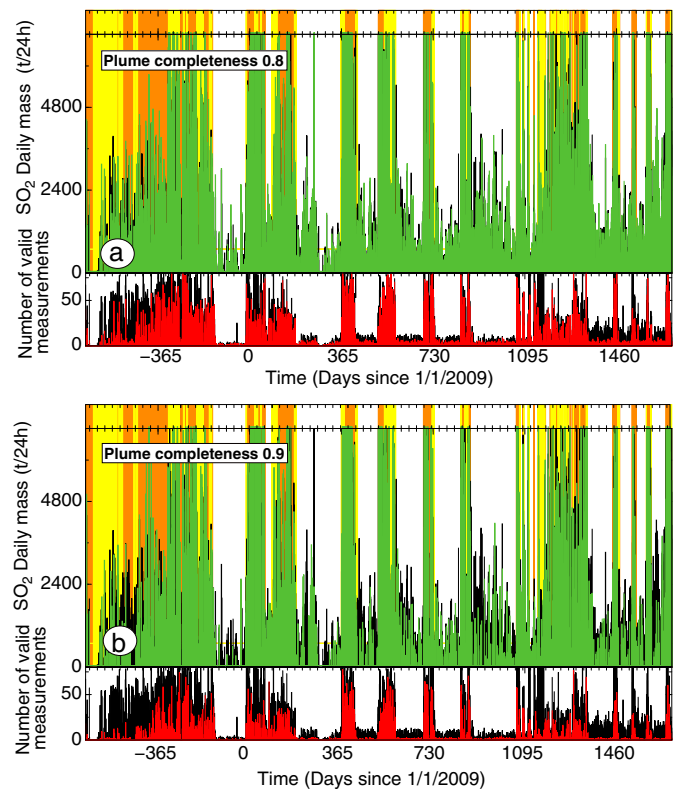


Fig. 3. SO₂ daily extrapolated emissions for Tungurahua volcano since January 2007 until August 2013. As for Fig. 2 orange, yellow and white background represent HEA, LEA and quiescence. a) SO₂ daily emission calculated using 0.5 (black bars) and 0.8 (green bars) plume completeness. Number of corresponding valid measurements during the day are in black for 0.5 and in red for 0.8. b) SO₂ emission calculated using 0.5 (black bars) and 0.9 (green bars) plume completeness. Number of corresponding valid measurements during the day are in black for 0.5 and in red for 0.9. Note that SO₂ emission for 0.5 and 0.8 plume completeness are very similar despite a slight reduction in the number of measurements, while for 0.9, the number of valid measurements is drastically reduced and for quiescence very few or no measurements are validated leading to zero emission.

3.2. Daily observed SO₂ mass

Alternately, in order to determine the daily observed mass of SO₂, we developed a procedure in which we integrate the highest available flux measurements among all stations. To achieve this, for each day, we scan the available time series between 07:00 and 17:00 (local time) searching for the highest fluxes (Fig. 4). However, NOVAC instruments do not provide regularly sampled time series, nor are they synchronized among the different instruments. This is because the durations of the individual scans vary depending on local light intensity. Time series may also be sparse because of invalidation of numerous complete scans where SO₂ was not detected. Therefore, to identify the highest fluxes we use a sliding search window with a variable duration. The window is shifted with no overlap and its length is adjusted according to the duration of the measurements. Starting at 07:00 with an arbitrary window duration of 5 min, we move the search window until we find flux measurements and determine the highest value among those acquired within the interval of the search window. As the highest value is selected, when two or more stations are able to see the plume, the method provides a potential correction for underestimated clouds-affected values. This highest flux is considered valid for the duration of the corresponding scan plus a constant inter-scan time, which depends on the instrument (between 0.9 and 2.5 min). The corresponding mass of SO₂ is calculated by multiplying the flux measurement by its corresponding duration of validity. The new search window size and shift are set to the last validity duration and the search is continued.

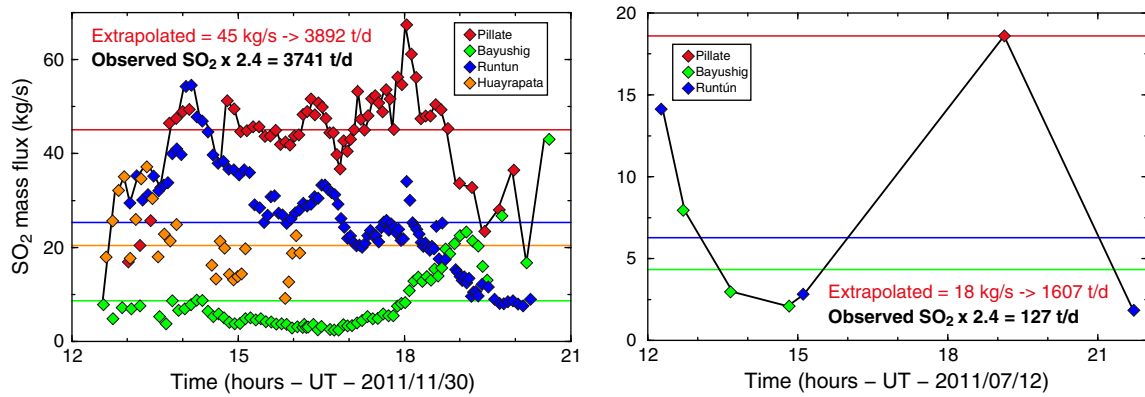


Fig. 4. Examples of individual SO_2 measurements at the 4 different stations. Coloured diamonds represent the valid individual SO_2 measurements at the 4 permanent DOAS stations on 30/11/2011 (left) and 12/07/2011 (right). The first day has a total of 291 valid measurements while the second has only 7. The daily average for each station is shown as a horizontal line of the same colour. A thick black line joins data points used to determine the daily observed mass of SO_2 . On 30/11/2011 extrapolated and observed $\text{SO}_2 \times 2.4$ are roughly equivalent, while on 12/07/2011 the extrapolation method clearly overestimates the total SO_2 emission.

Repeating this procedure for the whole period of daylight and adding the retrieved masses produce an estimate of the daily mass of SO_2 observed by the monitoring instruments.

This approach is different from those commonly used for reporting daily mean emission rates, as we do not extrapolate the available flux measurements to estimate a daily SO_2 mass for 24 h but only consider the observed masses to obtain a cumulative estimate which can be expressed in tons per ten hours (t/10 h). The underlying assumption is that the absence of measurements means the absence of SO_2 emissions from the volcano. Because this assumption is not strictly correct, our estimated masses might underestimate the real amount of SO_2 emitted during the 10 h of daily measurement. However, this approach corrects for the improper extrapolation of a reduced number of data points, as what often occurs during periods of low activity. In order to obtain a value over a full day (t/d or t/24 h) that is comparable with the extrapolated data, we can multiply the daily observed mass of SO_2 by 2.4, given that the stations work at Tungurahua for 10 h.

Comparing both resulting series leads to different SO_2 emission histories (Fig. 5). While SO_2 emissions during eruptive phases are globally equivalent using both methods, degassing during quiescence episodes (passive degassing) is drastically reduced by the daily observed mass method and in consequence the total SO_2 emission is also lowered.

During quiescent phases at Tungurahua only sporadic gas plumes or intense fumarolic activity is observed, hence degassing is a transient process. In consequence, extrapolating few flux measurements as representative of the whole day SO_2 emission while transient degassing behaviour dominates, leads to over-estimated values. Fig. 6 shows the cumulative SO_2 curves produced by the conventional method (Extrapolated), the proposed method (Observed masses) and the 24 h extrapolation of the proposed method (Observed masses multiplied by 2.4). The first curve reaches a high value of 2.50 Mt of SO_2 emitted by the volcano since 2007, while a cumulative mass of 0.52 Mt was observed, corresponding when multiplied by 2.4 to a total of 1.25 Mt of SO_2 . This last curve reflects well the periods of SO_2 emission by changes in the slope. Flat segments represent quiescence periods, light slope long periods of continuous/sub-continuous activity (periods 1 and 3) and high slopes represent shorter phases of activity (periods 2 and 4).

3.3. Car based traverses

In order to corroborate the results obtained with the permanent network, we have performed Mobile DOAS traverses, especially during periods of high activity. Our Mobile DOAS system consists of a mini-USB2000 OceanOptics spectrometer coupled to a zenith-viewing

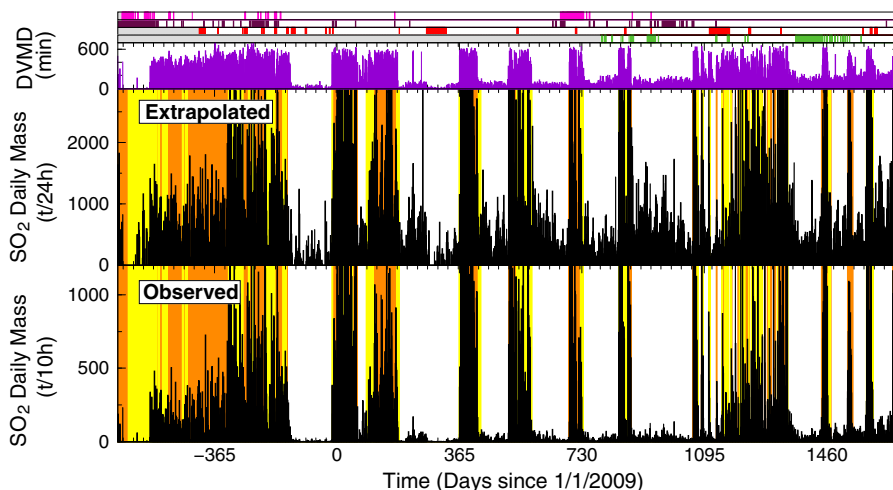


Fig. 5. Comparison between extrapolated (upper plot) and observed (lower plot) daily SO_2 mass measurements for the period between February 2007 and August 2013. Note that extrapolated SO_2 is expressed in tons per 24 h while observed SO_2 is expressed in tons per 10 h. Vertical scales have been scaled by a factor 2.4 to be comparable. Violet histogram shows the daily validated measurement duration (DVMD). The 4 upper lines indicate downtime periods for the DOAS stations: Pillate (red), Huayrapata (maroon), Bayushig (magenta) and Runtun (green) with grey indicating periods when the stations were not yet installed. Equivalent fluxes in kg/s are shown in Appendix B as Supplementary Material 1.

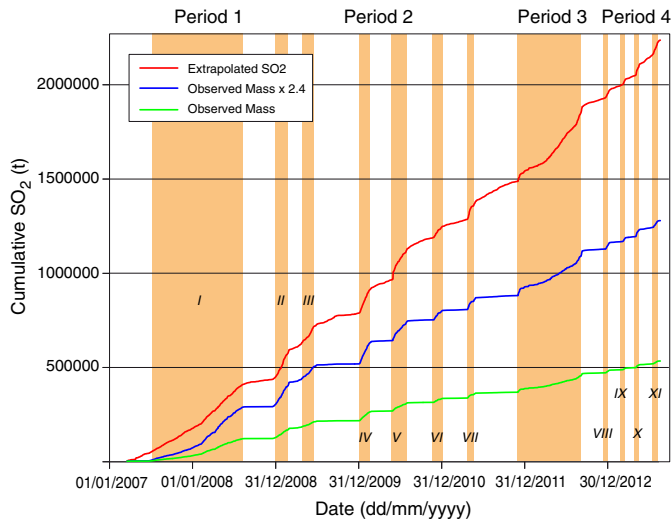


Fig. 6. Cumulative curves of SO_2 emission using extrapolated values, observed masses and observed masses multiplied by 2.4. Eruptive phases are marked in orange.

telescope by a quartz fibre. To acquire and process the spectra we used the Mobile-DOAS v.5 software by Zhang and Johansson (2009). An external GPS antenna provides precise location and time in order to calculate the integral of the flux across the section of the plume. Usually 4 to 6

traverses are done in one day through the Baños–Penipe route, to the west of the volcano (Fig. 1).

Mobile DOAS data are processed using the same source of wind velocity as for the processing of data from the permanent stations. Wind direction is deduced directly from the traverse, and plume height is not necessary (at least not directly, since it is required to retrieve the wind speed at the altitude of the plume). Completeness of the plume is assured for traverses in most of the cases. Traverses tend to give higher columns than scanning measurements, highlighting the effect of dilution due to scattering of radiation below the plume. This effect is more pronounced for measurements taken from the scanners due to their greater distance from the source. However, globally, the fluxes obtained by Mobile DOAS coincide (within uncertainties) with those provided by the permanent stations (Fig. 7). The better similarity between the traverses and the extrapolated or observed daily estimates depends on the representativeness of the traverses in reference with the overall daily degassing as well as on the stability of the degassing during the day.

4. Types of activity

We distinguish three types of activity during the 2007–2013 period: (1) Quiescence, (2) Low explosive activity and (3) High explosive activity (Fig. 2). This distinction is based on the seismo-acoustic recordings and activity reports from the Tungurahua Volcano Observatory (OVT) (<http://www.igepn.edu.ec>). The seismo-acoustic records allow differentiating between periods with only Strombolian-type activity and periods when Vulcanian-type outbursts also occur. This distinction is done by quantifying the intensity of infrasound radiation emitted during

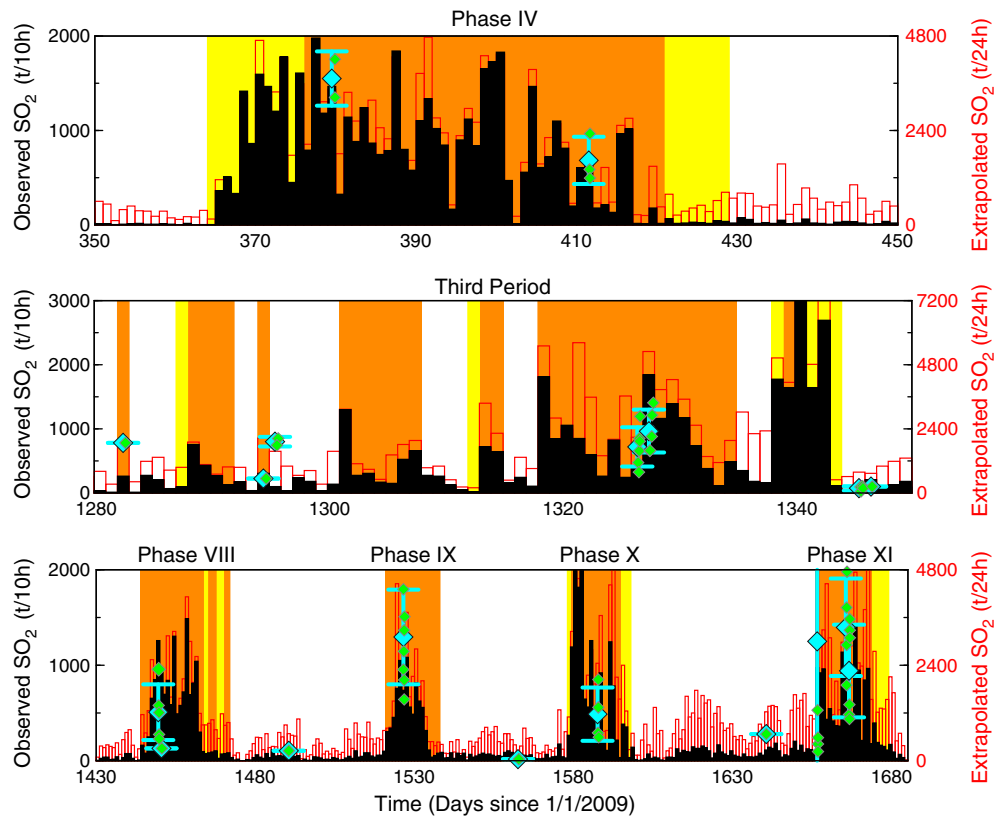
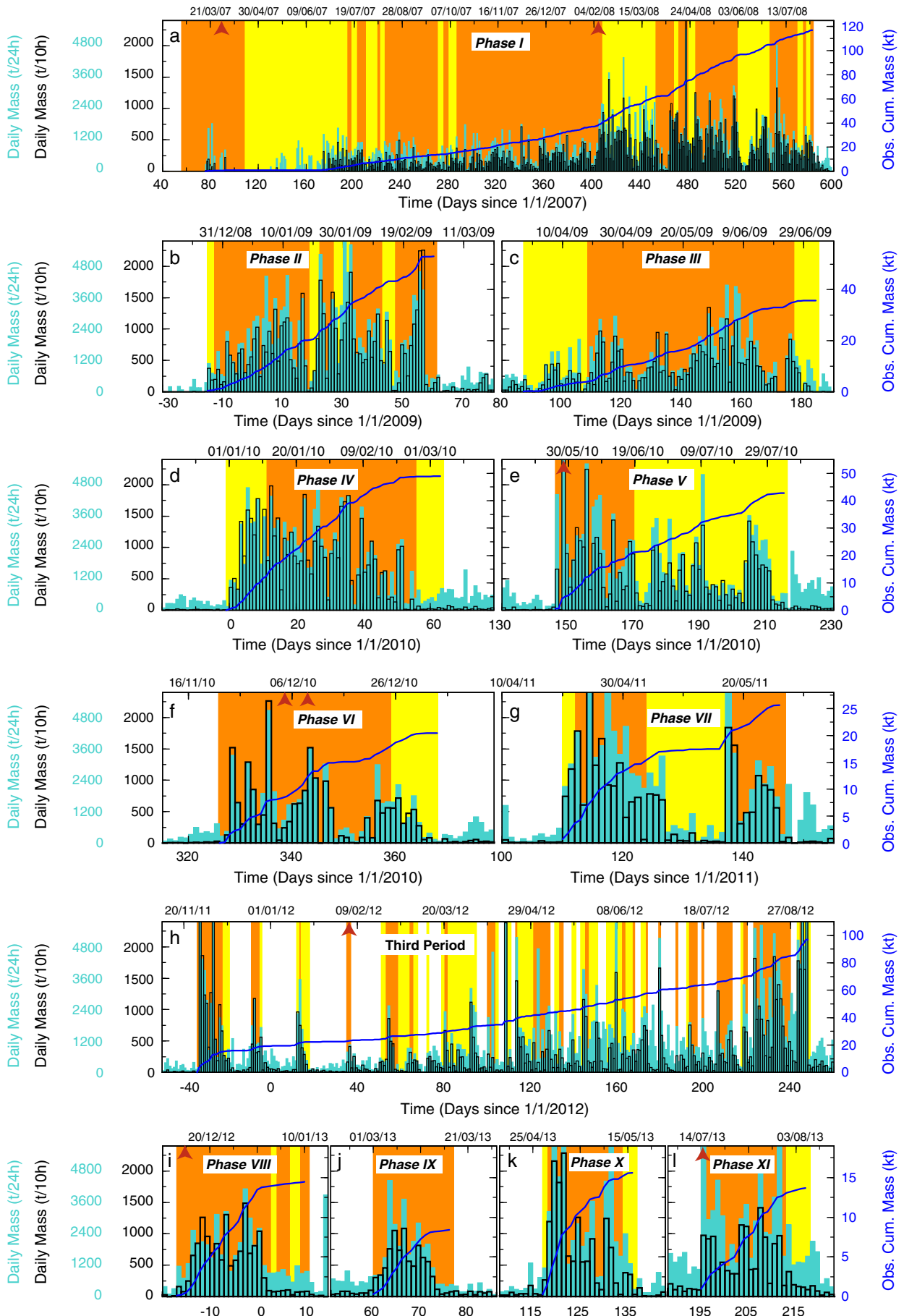


Fig. 7. Comparison between SO_2 estimates obtained doing mobile-DOAS traverses and those obtained from the DOAS permanent network. Estimates from the permanent network are shown as black filled histograms for observed masses in tons per 10 h and as empty red histograms for the extrapolated measurements expressed in tons per 24 h. Note that vertical scale for observed masses has been scaled by a factor 2.4 to be comparable with extrapolated masses. Light blue diamonds represent Mobile-DOAS average daily SO_2 measurements expressed in tons per 24 h and green diamonds individual measurements. Observed masses, when multiplied by a factor of 2.4, are consistent during eruptive phases with the extrapolated DOAS and Mobile DOAS values.



explosions. Using a network of 4 infrasound sensors located between 5 and 7 km from the vent (Kumagai et al., 2010), we normalize the peak-to-peak pressure amplitude at each station to a distance of 1 km from the source and calculate the average over the 4 stations (Steele et al., 2014). We then consider Vulcanian explosions to be those whose mean acoustic excess pressure is ≥ 100 Pa at a distance of 1 km, as consistent with Johnson (2003). The observatory reports complete the description of surface phenomena associated with each type of activity.

4.1. Quiescence

Quiescence is characterized by a complete absence of eruptive activity or only the presence of weak fumaroles in the crater and the upper part of the cone or sporadic gas plumes. Such manifestations generally reach heights less than 200 m above the crater rim and exceptionally, up to 500 m according to OVT reports. During quiescence neither juvenile pyroclasts nor lava is emitted from the vent. Episodes of repose last from 26 to 184 days, except during the third period of activity when very short quiescence time intervals were observed (between 3 and 17 days). Seismic activity is weak during such periods with only a few long period and volcano-tectonic earthquakes.

4.2. Low explosive activity

Low explosive activity (LEA) is characterized by ash and gas emissions with low-energy explosions (< 100 Pa, i.e. Strombolian) and/or small short-lasting fountains of incandescent ejecta (< 500 m above the crater rim). Ash columns vary from a few hundred metres up to 3 km in height with variable ash content. Persistent ash columns can last for hours and even days, producing abundant ash fallouts. These emissions are generally accompanied by a rumbling noise yet infrequently show completely silent degassing behaviour. Small rockfalls and short-runout avalanches (< 1 km) of accumulated pyroclastic material have been observed on several occasions during this type of activity. The seismic signals recorded during LEA are mainly numerous small explosion quakes, long period events and tremor (occasionally harmonic). This type of activity can be considered in general as Strombolian style. No Vulcanian-type explosion is present during these episodes.

4.3. High explosive activity

High explosive activity (HEA) is defined primarily by the presence of high-energy (> 100 Pa, i.e. Vulcanian) explosions that are usually accompanied by a canon shot-like sound heard in nearby areas and during the most intense outbursts, up to 30 km from the vent. The eruptive columns usually vary in height between 1 and 4 km above the crater rim yet may reach 8–10 km during paroxysmal events. At night time, fountains or incandescent ejecta reaching up to 1 km above the crater rim have been observed. Incandescent blocks usually remain within 2 km distance of the vent however, ballistic projectiles were observed up to 3.5 km away during a very high-energy explosion event recorded on the 14 July 2013. The ash content is generally high producing dark grey to black eruptive columns associated with intense ash falls. During some paroxysmal phases pyroclastic flows were also produced either by long-lasting fountains (6 February 2008, 4 December 2010) or triggered by high-energy Vulcanian explosions (27 March 2007, 28 May 2010, 16 December 2012, 14 July 2013). These pyroclastic flows reached

distances 3 to 6.5 km from the vent. The seismic signals recorded during high explosive activity are large explosion quakes with very-long period components and N-shaped acoustic signals, long period events, harmonic and emission tremors, and volcano-tectonic earthquakes. We relate this type of eruptive activity to a Vulcanian style, alternated with more or less violent Strombolian episodes.

5. Eruptive activity and SO₂ degassing since 2007

Given that the first DOAS-NOVAC stations were installed in February 2007, the record of SO₂ emissions for the previous period is not detailed in this paper. Between February 2007 and August 2013, eleven well-defined eruptive phases have been recognized within four main periods of activity (Fig. 2). The first period consists of a long lasting activity phase (Phase I) where LEA and HEA are intercalated. A doubling of the SO₂ emission is seen since day 400 (Fig. 8a). This increase in daily mass is observed after the February 2008 paroxysm, probably indicating the arrival of a magma richer in SO₂. A progressive decrease in the SO₂ emission is observed towards the end of the phase. No clear change in daily SO₂ emission is observed linked to HEA or LEA. The second period comprises 6 activity phases lasting from 37 to 98 days (Fig. 8b, c, d, e, f and g). The first phase of this period, Phase II, still displays an alternation of HEA and LEA, while the others display mostly LEA episodes at the beginning and/or at the end of the phase. In these phases globally daily SO₂ emission is lower for LEA episodes than for HEA, displaying a low slope in the cumulative mass curve or even producing a flat line (end of phases III, IV, V and VI). Phases V and VI begin directly by HEA, which in both cases was characterized by a sudden opening of the conduit by Vulcanian explosions leading to the formation of pyroclastic flows. For the other phases of the second period the activity increases progressively, without pyroclastic flows forming explosions. Third period is characterized by an almost continuous activity and the distinction of clear individual phases is difficult (Fig. 8). HEA is observed at the beginning of the period with a rapid increase in daily SO₂ emission. An alternation of HEA–LEA and quiescence is observed with a cumulative SO₂ curve whose slope increases progressively until the end of the period where higher emission is recorded. The fourth period comprises four activity phases lasting between 17 and 28 days (Fig. 8i, j, k and l). Phases VIII, IX and XI begin directly by a HEA with Vulcanian explosions, which formed pyroclastic flows only for phases VIII and XI. Despite the HEA beginning of phase IX, the increase in the activity and degassing is progressive, as well as the decrease towards the end, forming a bell-shaped distribution for SO₂. Phase X begins by only one day of LEA and a rapid increase in SO₂ degassing is recorded at the beginning of the phase to also gradually decrease to almost zero SO₂ degassing when activity fades out. Again LEA episodes display an almost flat SO₂ cumulative curve indicating a lower daily SO₂ emission for these episodes as compared to HEA. This is shown in Table 1, which summarizes the main characteristics of each phase. Indeed, for the first and third periods, when activity is more or less continuous, the SO₂ emission associated to LEA or HEA episodes is very similar. For phases of the second and fourth periods HEA episodes display higher SO₂ emission than LEA episodes (Table 1). Quiescence episodes are characterized by low SO₂ daily observed masses, despite the fact that in some cases SO₂ extrapolated emission (shown in turquoise in t/24 h in Fig. 8) might be as high as for the activity phases. Detailed description of each eruptive phase is available in Appendix B as Supplementary Material 2.

Fig. 8. Comparison between SO₂ observed masses (black bars) and SO₂ extrapolated masses (turquoise bars) during each eruptive phase since 2007. Daily observed masses are expressed in tons per ten hours and extrapolated masses are expressed in tons per 24 h with separate vertical scales on the left of the plots. The vertical scale for the observed masses is 2.4 times smaller so that curves are directly comparable. White background indicates periods of quiescence. Yellow and orange represent low (LEA) and high explosive activity (HEA) respectively. Cumulative SO₂ emission based on observed masses (in t/10 h) is shown as a thick blue line. Time scale is indicated in number of days since January 1 for each year at the bottom of each diagram and calendar dates are indicated at the top. The different plots a) to l) correspond to the phases of activity described in Table 1 and the Supplementary Material. During the HEA and most of the LEA episodes SO₂ observed masses (multiplied by 2.4) are fairly the same as the SO₂ extrapolated masses. During quiescence SO₂ observed masses are much lower than the corresponding extrapolated mass. Red arrows indicate the days when long run-out pyroclastic flows were produced.

Table 1
Summary of the main characteristics of each eruptive phase since February 2007. "Beginning of the phase" refers to the type of onset. Sudden awakening of the volcano is typically characterized by a strong Vulcanian eruption with intermediate to long run-out pyroclastic flows. Progressive refers to an *in crescendo* increase in the intensity of the activity, mainly Strombolian in style. To describe the eruptive sequences we use L for low explosive activity (LEA), H for high explosive activity (HEA). Average and maximum plume heights were obtained from the Washington VAAC (<http://www.ssd.noaa.gov/VAAC/messages.html>), which is constructed from visual or satellite observations. The average SO₂ emission and total cumulated SO₂ calculated using the *observed masses* method are shown (t/10 h). For comparison with other volcanoes we also show in bold total values multiplied by 2.4. Average SO₂ emissions during HEA and LEA episodes for each phase and quiescence are also shown.

| Period | Phase | Start | End | Quiescence (days) | Duration (days) | Days with SO ₂ data | Beginning of the phase | Eruptive sequence | Plume height above the crater average (max) (km) | Pyroclastic flows (type, # valley affected, minimum runout) | Number of significant explosions | SO ₂ daily average observed mass (t/10 h) and × 2.4 | Cumulative SO ₂ (kt) Observed mass and × 2.4 | SO ₂ range observed mass (t/10 h) and × 2.4 | SO ₂ average HEA (observed mass t/10 h) and × 2.4 | SO ₂ average LEA (observed mass t/10 h) and × 2.4 | Quiescence SO ₂ average (observed mass t/10 h) and × 2.4 |
|----------|-------|----------|----------|-------------------|-----------------|--------------------------------|------------------------|---------------------|--|---|----------------------------------|--|---|--|--|--|---|
| Period 1 | I | 24/02/07 | 04/08/08 | 68 | 527 | 417 | Progressive | Alternance H-L (25) | 2.7 (9.4) | 27/03/2007 (explosion, 1 valley, 1 km) 06/02/2008 (column collapse, 3 valleys, 5 km) | 1763 | 281 ± 278 674 ± 667 | 120.4 288.96 | 1.4–1747 3.3–4193 | 212 ± 243 509 ± 482 | 276 ± 282 662 ± 677 | 15 ± 42 36 ± 101 |
| Period 2 | II | 16/12/08 | 01/03/09 | 132 | 76 | 76 | Progressive | Alternance L-H (10) | 2.6 (5.2) | | 377 | 698 ± 512 1675 ± 1229 | 55.3 132.72 | 3.3–2386 7.8–5727 | 584 ± 603 1402 ± 1447 | 352 ± 325 845 ± 780 | 50 ± 62 120 ± 149 |
| | III | 28/03/09 | | 26 | 98 | 92 | Progressive | L-H-L | 2.3 (6.1) | | 212 | 389 ± 289 934 ± 694 | 37.6 90.24 | 0.32–1324 0.76–3177 | 393 ± 318 943 ± 763 | 139 ± 157 334 ± 377 | 15 ± 23 36 ± 55 |
| | IV | 30/12/09 | | 179 | 65 | 65 | Progressive | L-H-L | 2.5 (5.5) | | 521 | 753 ± 581 1807 ± 1394 | 49.8 119.52 | 2.5–1872 5.98–4493 | 593 ± 548 1423 ± 1315 | 501 ± 672 1202 ± 1613 | 20 ± 18 48 ± 67 |
| | V | 26/05/10 | 03/08/10 | 82 | 70 | 70 | Sudden | H-L | 2.9 (8.8) | 28/05/2010 (explosion, 6 valleys, 4.5 km) | 1351 | 611 ± 566 1466 ± 1358 | 43.3 103.92 | 1.34–2356 3.23–5655 | 599 ± 658 1438 ± 1579 | 356 ± 372 854 ± 893 | 20 ± 19 48 ± 46 |
| | VI | 22/11/10 | 03/01/11 | 110 | 43 | 42 | Progressive | H-L | 2.7 (5.5) | 04/12/2010 (column collapse, 8 valleys, 4 km) 09/12/2010 (explosion, 1 valley, 3 km) | 111 | 487 ± 490 1169 ± 1176 | 20.9 50.16 | 1.24–2399 2.98–5758 | 411 ± 562 986 ± 1345 | 285 ± 272 684 ± 653 | 18 ± 16 43 ± 38 |
| | VII | 20/04/11 | 26/05/11 | 106 | 37 | 37 | Progressive | L-H-L-H | 3.5 (7.3) | | 64 | 692 ± 627 1661 ± 1505 | 26.4 63.36 | 4.64–2638 11.13–6330 | 720 ± 546 1728 ± 1310 | 411 ± 546 986 ± 1310 | 25 ± 22 60 ± 53 |
| Period 3 | | 27/11/11 | 9/4/2012 | 184 | 283 | 282 | Progressive | Alternance L-H | 3.3 (7.3) | 04/02/2012 (explosion, 1 valley, 3 km) | 194 | 344 ± 537 826 ± 1289 | 102.1 245.04 | 1.4–4489 3.27–10773 | 484 ± 583 1162 ± 1399 | 416 ± 732 998 ± 1757 | 39 ± 40 94 ± 96 |
| Period 4 | VIII | 14/12/12 | 10/01/13 | 101 | 28 | 28 | Sudden | H-L-H-L-H | 2.8 (7.3) | 16/12/2012 (explosion, 4 valley, 3.5 km) | 453 | 517 ± 438 1241 ± 1051 | 14.8 35.52 | 7.42–1577 17.8–3874 | 465 ± 478 1116 ± 1147 | 61 ± 30 146 ± 72 | 41 ± 32 98 ± 77 |
| | IX | 01/03/13 | 17/03/13 | 49 | 17 | 17 | Progressive | H | 2.2 (3.3) | | 118 | 494 ± 328 1186 ± 787 | 8.6 20.64 | 8.5–876 20.3–2102 | 326 ± 293 782 ± 703 | | 54 ± 32 130 ± 77 |
| | X | 27/04/13 | 16/05/13 | 41 | 20 | 20 | Progressive | L-H-L | 2.0 (4.9) | | 151 | 780 ± 682 1872 ± 1637 | 16.3 39.12 | 24.6–2254 59.0–5408 | 936 ± 747 2246 ± 1793 | 177 ± 161 425 ± 386 | 74 ± 52 178 ± 125 |
| | XI | 14/07/13 | 05/08/13 | 58 | 23 | 23 | Sudden | H-L | 3.8 (8.8) | 14/07/2013 (explosion, 4 valleys, 6.5 km) | 64 | 596 ± 387 1430 ± 929 | 14.4 34.56 | 16.1–1548 38.6–3716 | 498 ± 430 1195 ± 1032 | 205 ± 129 492 ± 310 | |

6. Discussion

6.1. Passive vs. explosive degassing

Arellano et al. (2008) highlight the dominance of passive degassing at Tungurahua volcano for the eruptive period between 1999 and 2006. Indeed, while the SO₂ emission related to explosive activity showed higher daily values, the cumulated SO₂ emission recorded during low activity and quiescence is higher, accounting for up to 90% of the total emission of SO₂. Our analysis of the effect of the calculation method for the daily SO₂ emission and the differences in defining the explosive degassing could explain partially the outnumbering of passive over explosive SO₂ degassing during the mentioned period but certainly not all of it. Arguably, since late 2008, the general behaviour of Tungurahua volcano has changed, and quiescence episodes have become more common and longer (Fig. 2). During HEA and most of the LEA episodes, the two methods of estimation, the daily extrapolated emission (1.60×10^9 kg) and the *daily observed masses* multiplied by 2.4 (1.2×10^9 kg), produce results within the same range. In both, the periods with higher SO₂ emissions coincide with the periods of overall volcanic activity (Figs. 5 and 8). On the contrary, when observing the results for quiescence phases, the extrapolated daily emission method displays much higher values than the observed ($\times 2.4$) daily masses method (Figs. 6 and 8). This is expected because the extrapolated values globally overestimate the actual SO₂ emission, particularly when there are few valid measurements per day, which correspond mainly to sporadic gas emissions not representative of the whole degassing behaviour during a whole day. Nevertheless, this fact has important implications for the quantification and understanding of passive degassing. The total cumulative SO₂ emission during quiescence phases calculated by the extrapolation method is 5.9×10^8 kg, while using the observed masses ($\times 2.4$) method the total SO₂ emission is 7.5×10^7 kg, i.e. one order of magnitude lower. According to the observed masses multiplied by 2.4, the percentage of SO₂ released during quiescent phases yields only 5% of the total degassing, with a daily average mass of 73 ± 56 t/d. Calculating the mass of magma involved in the eruptive period since 2007 using the different cumulative SO₂ emission values would lead to extremely different volumes of magma sustaining the activity. Considering the SO₂ emission obtained by the observed masses method, passive degassing has almost disappeared at Tungurahua since late 2008, reflecting a change in eruptive dynamics of the volcano. We propose that Tungurahua has changed from open vent activity, allowing almost continuous passive degassing, as for example Fuego in Guatemala (Lyons et al., 2010) or Popocatepetl in Mexico during fumarolic or effusive periods (Delgado-Granados et al., 2001), to a more episodic activity reflecting a partially closed system with occasional plugging of the conduit with low SO₂ degassing during quiescence.

6.2. Open vent vs. closed vent system: implications on the activity of Tungurahua volcano since 2008

Samaniego et al. (2011) proposed that episodic injections fed magma to a modest reservoir 10 km below Tungurahua's crater, which in turn supplied magma to the surface between 1999 and 2005. The authors associate the intermittent enhanced explosive activity to these magma injections, but ash and gas emission activity was globally persistent (Arellano et al., 2008). During this period, variable magma supply rates explain the transition between Vulcanian and Strombolian styles (Wright et al., 2012). Bulk-rock composition of Tungurahua ashes did not change during the 1999–2005 period, indicating a chemically and probably physically homogeneous reservoir despite the different magmatic injections (Samaniego et al., 2011). Seven periods of quiescence were observed lasting between 8 to 94 days between 1999 and 2004 and a long quiescence of 353 days in 2005. Nevertheless, in all cases volcanic unrest was progressive with a clear escalating

number of VT and/or LP earthquakes before equally escalating surface manifestations.

Since 2007, the long phases of activity (Periods 1 and 3) have been characterised by dominantly Strombolian activity. During those phases, SO₂ degassing has increased progressively and varied according to the intensity of the observed surface activity. This behaviour is similar to that observed until 2005 and comparable to Popocatepetl until 2000, when activity was also more-or-less continuous (Delgado-Granados et al., 2001; Arciniega-Ceballos et al., 2003). These long periods of activity display a low slope in the relation between total cumulative SO₂ emission and the duration of the phase (Fig. 9). The daily average SO₂ observed mass multiplied by 2.4 during these long phases is 735 ± 969 t/d. On the contrary, the short duration phases display a higher slope in such relation (Fig. 9). During these short phases (Periods 2 and 4) the daily average SO₂ observed mass multiplied by 2.4 is of 1424 ± 1224 t/d, almost twice as for long phases. These values are in the lower range of those observed in other andesitic volcanoes (Shinohara, 2008). Two contrasting behaviours are observed: a) progressive increase of degassing and ash venting with or without significant explosions at the beginning of the phase, and a dominant Strombolian-like activity (Phases II, III, IV, VII, IX, X); and b) sudden or very rapid increase in the activity simultaneous to or followed by the increase in SO₂ emission. This last activity usually begins with small Phreatic or Vulcanian explosions followed by a more energetic Vulcanian explosion producing pyroclastic flows, one or two days later. Then, a progressive or oscillating decrease of the activity's intensity and SO₂ degassing is observed (Phases V, VI, IX, XI). The difference between a) and b) is the onset of the eruptive phase, which should be controlled by the conditions at the vent. In the first case, some permeability in the conduit should exist to allow a progressive gas escape that inhibits the buildup of overpressure, leading to an *in crescendo* activity pattern, typical of an open vent system. On the contrary, for the second case, sealing of the conduit seems more effective, building an important gas overpressure and producing the more energetic and violent Vulcanian explosions that ultimately open the system. This change would depend on several conditions inherent to the magma itself, like its chemical composition, viscosity, temperature and volatiles and crystal content; or related to the feeding and plumbing system (Sparks, 2003). An increase in viscosity coupled with a decrease in temperature or associated with a change in magma composition could be responsible for reducing magma permeability producing a progressive sealing of the conduit, leading ultimately to the formation of a plug and in consequence to a closed system behaviour. A detailed geochemical study of the juvenile products should be done to test this hypothesis, which is beyond the scope of this study. A lower feeding rate and/or smaller volumes of injected magma can also lead to the plugging of the system by allowing more heat loss leading to fractional crystallisation and a viscosity

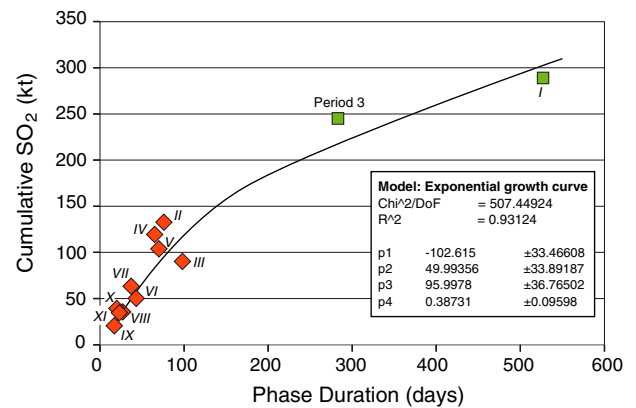


Fig. 9. Total released observed mass of SO₂ multiplied by 2.4 for each phase of activity plotted as a function of phase duration. Results from the model presented in the Appendix A and discussed in Section 6.4 are given in the inserted box.

increase (Cashman and Blundy, 2000). Once the vent is open, the activity would change to more Strombolian-like style or continue with lower energy Vulcanian explosions. Short activity phases have been observed in other andesitic volcanoes, like Ruapehu and recently Popocatepetl, but the periods of quiescence in those cases seem longer (months to years) (Nakagawa et al., 1999; Arciniega-Ceballos et al., 2003). According to the relatively small size of the recent eruptions ($VEI = 1$; Bernard et al., 2013), it seems that the critical volume of magma required to trigger an eruption can be built up faster.

6.3. Progressive vs. sudden onset of eruptive activity: implications on risk assessment

During the phases in which a progressive increase of activity is observed and Strombolian eruptive style is dominant, ash fallout is the main hazard for local populations. In the short-term, the major impact of this phenomenon occurs on the cattle and crops growing around the volcano, which constitute the main economic activity for nearby residents. In the long-term, ash fallout might have an important impact on human health depending on the duration of exposure but also on the ash composition (Horwell and Baxter, 2006). However, the ash from Tungurahua does not contain quartz or its polymorphs, reducing the potential risk for developing respiratory chronic diseases. Exceptionally small pyroclastic flows are observed during this kind of activity; nevertheless, they are too small to reach populated areas. The progressive evolution of these eruptive phases allows the local authorities and population to implement risk assessment plans and take actions to protect the cattle and water supply.

On the contrary, during phases where a violent Vulcanian eruption opens the vent, the related hazards are much greater. Typically pyroclastic flows able to reach populated areas are produced during this kind of events. In May 2010, July 2013 and more recently in February and April 2014 (not included in this study), pyroclastic flows killed cows and destroyed some farming zones on the flanks of the volcano. The travel time for these phenomena to reach the Baños–Penipe road is approximately 6 to 19 min (Hall et al., 2013). This leaves a very short time to emit an early warning and evacuate people living on the flanks of the volcano. Besides, the eruptive columns produced during these eruptions have reached up to 9 km above the summit, leading to ash plumes that can travel great distances, affecting larger areas. As an example, the ash plume from the 28 May 2010 eruption arrived at the city of Guayaquil (~180 km) in about 2 h and produced ash fallout that resulted in the temporary closure of the airport. Few or no precursory signs are typically detected before this kind of activity, creating a challenge to forecast these phenomena. As these violent eruptions without precursory signs are observed since 2010 at Tungurahua and more frequently during 2013–2014, new risk assessment plans should be created and implemented in the area to better protect human lives, livestock, and economic resources.

6.4. Relation between cumulative emission and duration of each phase

The relation observed in Fig. 9 between the cumulative emission of SO_2 and the duration of each phase of activity suggests that the magmatic system at Tungurahua follows an exponential growth of discharge. As first pointed out by Wadge (1981) for the case of basaltic systems, and expanded in more detail by e.g. Huppert and Woods (2002) or Mastin et al. (2008), who applied the model to the effusive activity of Mount St. Helens, this response occurs due to two main conditions: i) that the mass effusion rate is linearly related to the reservoir pressure; and, ii) that the magma-reservoir pressure is linearly related to the mass of magma in the reservoir (the difference between erupted and intruded magma). On the other hand, a logarithmic curve of growth is expected for systems where magma flow is controlled by rate-dependent frictional resistance, e.g., in lava dome eruptions. This interpretation should however be taken only for its heuristic value, since

several uncertainties of the actual conditions at Tungurahua remain large. For this study, the most important question is to what extent the mass emission rate of SO_2 can be used as a proxy for the mass eruption rate? The factors controlling this dependence are: the initial sulphur content of the magma, the speciation of S between SO_2 and any other S-bearing species and the partition coefficient of SO_2 between the gas and melt phases. Finally, there is the measurement uncertainty of SO_2 in the plume, including all possible transformations (scrubbing, deposition, chemistry, radiative transfer effects, etc.) after emission. All these factors can change with time, making difficult to assign a one-to-one correspondence between SO_2 and magma discharge. But the type of relation observed in this case is just what is expected for an elastic reservoir, indicating that degassing-induced decompression of the magmatic system may well define the intensity and duration of the eruptive phases.

The model is proposed to account for a simple physical mechanism behind the clear observation, presented in Fig. 9, that the cumulative emission of SO_2 for each phase of activity is not linearly scaled with the duration of its corresponding phase. Short-duration periods of activity tend to have larger intensity of emission than long-duration periods. This led us to believe that our observations support the intuitive notion that degassing is related to depressurization of the magmatic system. Moreover, the application of this simple model permits an estimate of the characteristic time of discharge for the volcano $\sim 50 \pm 34$ days compared to a mean duration of the phases of activity of 79 ± 29 days and identifies a relatively small rate of magma intrusion during the discharge, which is consistent with the sporadic pattern of activity at Tungurahua. The mathematics of discharge of this system is identical to those representing the discharge of a simple capacitor-resistor electric circuit, providing a simple analogue to the magmatic system. More details are given in the Appendix A.

7. Conclusions

We developed a routine, which takes into account the measurements from all available DOAS stations and integrates the highest available measurements to estimate the daily masses of SO_2 recorded by the network during the 10 h of daily operation. For comparison purposes with other daily extrapolated measurements these “observed” masses can be multiplied by 2.4, or the equivalent factor depending on the operation time of the considered network to obtain daily emission amounts of SO_2 . This method strongly reduces the SO_2 emissions during quiescent phases producing an SO_2 time series well correlated with the eruptive activity. During the study period, 2007–2013, Tungurahua volcano changed its behaviour from a more-or-less continuously degassing volcano as observed between 1999 and late 2008 to a volcano having episodic activity without significant degassing during quiescence periods. Between February 2007 and August 2013, eleven well-defined phases of activity occurred, lasting from 17 to 527 days, interspersed with quiescence periods lasting from 26 to 184 days. Only between November 2011 and September 2012 (Period 3) the quiescence episodes were shorter giving an almost continuous activity. During the phases of activity, patterns of degassing are irregular in relation with eruptive patterns, which are also quite diverse. Nevertheless, globally high explosive activity (HEA) episodes show a higher SO_2 emission than low explosive activity (LEA) episodes. Eruptive phases may start violently with strong Vulcanian explosions accompanied by a sudden increase of SO_2 degassing or alternately the activity may rise progressively with a slow increase in SO_2 emissions. A total of 1.2×10^9 kg of SO_2 has been observed during the 1266 days of both LEA and HEA episodes recorded since 2007, comprising about 95% of the total emission during the studied period. For the short-lasting phases of activity, results show an almost linear relation between the duration of the phase and the emitted amounts of SO_2 . The long duration phases show a different trend indicating a lower daily emission. These two trends can be conciliated in a general simple model of elastic decompression of the

magmatic system, with a characteristic relaxation time commensurable with the typical duration of the eruptive phases. Our SO₂ time series show low to negligible SO₂ degassing during quiescence periods probably due to partial or total plugging of the conduit, which in turn leads to closed system behaviour. This interpretation is supported by the sudden and very explosive onsets observed on several occasions with few or no evident precursory signs making it more difficult to forecast the reactivation of the volcano. This impedes the issuing of early warnings and in consequence new risk assessment plans should be created and implemented in the area to better protect human lives and property.

Acknowledgements

Data for this study comes from the DOAS network at Tungurahua, which is co-financed by NOVAC (EU-PF6), SENESCYT – PIN08-IGEPN and BID 1707-OC-EC Projects. The classification of the explosions came from the JICA seismic and infrasound network. This research has been conducted in the context of the Laboratoire Mixte International “Séismes et Volcans dans les Andes du Nord” of IRD. The authors greatly acknowledge all the IG staff in charge of the monitoring of Tungurahua volcano, specially at the OVT. We would also like to thank Sonja Storm for compiling column heights from VAAC reports since 2007 and Pablo Samaniego for the insert in Fig. 1. The authors kindly acknowledge the comments from Thor Hansteen, Robin Campion and an anonymous reviewer, which greatly improve this manuscript, as well as the editorial handling by Alessandro Aiuppa.

Appendix A. Model of magma discharge of an elastic reservoir

Following Wadge (1981), Huppert and Woods (2002) and Mastin et al. (2008), an exponential growth curve of magma discharge is expected for a reservoir which overpressure $\Delta p = p - p_0$ is linearly related to the difference between recharged mass M_i and erupted mass M_e : $\Delta p = C(M_i - M_e)$. It can be shown that the constant $C = \frac{\partial p}{\partial M}$ depends on the reservoir and magma compressibilities, the magma density and the reservoir volume. A second assumption for an elastic reservoir is that mass emission rate Q_e is linearly related to reservoir pressure: $Q_e = Ap - B$, with constants A and B . The cumulative erupted mass can be integrated for constant mass recharge (see Appendix 2 in Mastin et al., 2008), giving:

$$M_e = \frac{(Ap_0 - B) - Q_i}{AC} (1 - e^{-ACt}) + Q_i t. \quad (A1)$$

For a discharging reservoir which has reached the necessary overpressure by accumulation of magma or other processes (crystallisation-induced degassing, tectonic stress, etc.) with no recharge, the rate of mass emission can be found to be equal to: $Q_e = (Ap_0 - B)e^{-ACt}$. The constants A , B and C are related to the physical variables defining the reservoir (initial overpressure, volume, compressibility), conduit (cross section, length) and magma (compressibility, density, viscosity). The details depend on the dynamic conditions of the flow and may indeed also change over time. In particular, the “characteristic time” of the discharge is $\tau = \frac{1}{AC}$.

For the case studied here, we performed a non-linear (Levenberg–Marquardt) regression analysis to fit the data in Fig. 9 to an expression of the form (A1). The characteristic time is found to be about 50 ± 34 days, compared to a mean duration of the phases of activity of 79 ± 29 days. The gas intrusion rate is found to be 0.38 ± 0.1 kt/d. For comparison, Champenois et al. (2014) estimated a net recharge rate of 7×10^6 m³/y at a depth of 11 km from modelling the large scale ground deformation at Tungurahua during 2003–2006. This recharge rate corresponds to about 50 kt/d of magma inflow rate, from which a (SO₂) gas/magma intrusion ratio of about 8000 ppm would be necessary to explain the observed extrusion rate at Tungurahua. It is well known

that Tungurahua exhibits ‘excessive’ SO₂ degassing (Arellano et al., 2008) of varying efficiency, which explains the rather large sulphur content in the magma that would be necessary to account for the observed emission, if all the gas emission would originate from the erupted magma alone.

The magma emission rate is related to the SO₂ gas emission rate through the relation:

$$M_e = M_{SO_2}^{measured} \left(\frac{M_{SO_2}^{gas}}{M_{SO_2}^{measured}} \right) \left[\left(\frac{M_e}{M_S} \right) \left(\frac{M_S}{M_S^{SO_2}} \right) \left(\frac{M_{SO_2}^{melt+gas}}{M_{SO_2}^{gas}} \right) \left(\frac{MW_{SO_2}}{MW_S} \right) \right]. \quad (A2)$$

Where each factor on the right side represents respectively the measured gas emission rate, the ratio between measured and emitted emission rate (related to measurement uncertainty), the sulphur content of the magma, the speciation of sulphur as SO₂, the partition coefficient of SO₂ between the melt and gas phases, and the ratio of molecular weights of S and SO₂. Some of these factors are controlled by dynamic processes and may not remain constant between different phases of activity, but their time-averaged values should not vary drastically for different phases of activity. Unfortunately, we lack detailed information to determine these factors for the magma of Tungurahua in the present study.

This simple model of discharge thus predicts the correct order of magnitude of the typical duration and recharge rate of the eruptive phases. This indicates that observing the trend of degassing gives indication of the relaxation of the magmatic overpressure leading the eruption. The above mathematical relations have the same form as the equation of discharge of a capacitor–resistor electric circuit, with the charge representing mass, voltage proportional to pressure and capacitance dependent on compressibility and other rheological properties of the magma–conduit–reservoir system.

Equation of the form: $y = p1e^{-\frac{x}{p2}} + p3 + p4x$, thus $p2$ is the characteristic time, and $p4$ the recharge rate (cf. Eq. A1, Fig. 9).

Appendix B. Supplementary data

Supplementary data to this article can be found online at <http://dx.doi.org/10.1016/j.jvolgeores.2015.03.022>.

References

- Allard, P., Malorani, A., Tedesco, D., Cortecchi, G., Turi, B., 1991. Isotopic study of the origin of sulphur and carbon in Solfatara fumaroles, Campi Flegrei caldera. *J. Volcanol. Geotherm. Res.* 48, 139–159.
- Andres, R.J., Kasgnoc, A.D., 1998. A time-averaged inventory of subaerial volcanic sulphur emissions. *J. Geophys. Res. – Atmos.* 103 (D19), 25251–25261.
- Arciniaga-Ceballos, A., Chouet, B., Dawson, P., 2003. Long-period events and tremor at Popocatepetl volcano (1994–2000) and their broadband characteristics. *Bull. Volcanol.* 65, 124–135.
- Arellano, S.R., Hall, M., Samaniego, P., Le Pennec, J.L., Ruiz, A., Molina, I., Yepes, H., 2008. Degassing patterns of Tungurahua volcano (Ecuador) during the 1999–2006 eruptive period, inferred from remote spectroscopic measurements of SO₂ emissions. *J. Volcanol. Geotherm. Res.* 176 (1), 151–162.
- Bernard, B., Bustillos, J., Wade, B., Hidalgo, S., 2013. Influence of the wind direction variability on the quantification of tephra fallouts: December 2012 and March 2013 Tungurahua eruptions. *Avances en Ciencias e Ingenierías 5–1*, A14–A21.
- Burton, M.R., Caltabiano, T., Murè, F., Salerno, G., Randazzo, D., 2009. SO₂ flux from Stromboli during the 2007 eruption: results from the FLAME network and traverse measurements. *J. Volcanol. Geotherm. Res.* 182 (3–4), 214–220.
- Casadevall, T.J., Rose, W.I., Gerlach, T.M., Greenland, L.P., Ewert, J., Wunderman, R., Symonds, R.B., 1983. Gas emissions and the eruption of Mount St. Helens through 1982. *Science* 221, 1383–1385.
- Cashman, K., Blundy, J., 2000. Degassing and crystallization of ascending andesite and dacite. *Philos. Trans. R. Soc. Lond.* 358 1770, 1487–1513. <http://dx.doi.org/10.1098/rsta.2000.0600> 1471–2962.
- Champenois, J., Pinel, V., Baize, S., Audin, L., Jomard, H., Hooper, A., Alvarado, A., Yepes, H., 2014. Large-scale inflation of Tungurahua volcano (Ecuador) revealed by persistent scatterers SAR interferometry. *Geophys. Res. Lett.* 41, 5821–5828. <http://dx.doi.org/10.1002/2014GL060956>.

- Conde, V., Bredemeyer, S., Duarte, E., Pacheco, J., Miranda, S., Galle, B., Hansteen, T., 2013. SO₂ degassing from Turrialba Volcano linked to seismic signatures during the period 2008–2012. *Int. J. Earth Sci. (Geol. Rundsch.)* 1–16.
- Daag, A., Tubianosa, B., Newhall, C., Tungol, N., Javier, D., Dolan, M., de los Reyes, P.J., Arboleda, R., Martinez, M., Regalado, M.T.M., 1994. Monitoring sulphur dioxide emissions at Mount Pinatubo. In: Punongbayan, R.S., Newhall, C.G. (Eds.), *The 1991–1992 Eruptions of Mount Pinatubo, Philippines*. U.S. Geological Survey Professional Paper.
- Delgado-Granados, H., Cárdenas González, L., Piedad Sánchez, N., 2001. Sulphur dioxide emissions from Popocatepetl volcano (Mexico): case study of a high-emission rate, passively degassing erupting volcano. *J. Volcanol. Geotherm. Res.* 108, 107–120.
- Douillet, G.A., Tsang-Hin-Sun, È., Kueppers, U., Letort, J., Pacheco, D.A., Goldstein, F., Aulock, F., Lavallée, Y., Hanson, J.B., Bustillos, J., Robin, C., Ramón, P., Hall, M., Dingwell, D., 2013a. Sedimentology and geomorphology of the deposits from the August 2006 pyroclastic density currents at Tungurahua volcano, Ecuador. *Bull. Volcanol.* 75 (11). <http://dx.doi.org/10.1007/s00445-013-0765-7>.
- Douillet, G.A., Pacheco, D.A., Kueppers, U., Letort, J., Tsang-Hin-Sun, È., Bustillos, J., Hall, M., Ramón, P., Dingwell, D., 2013b. Dune bedforms produced by dilute pyroclastic density currents from the August 2006 eruption of Tungurahua volcano, Ecuador. *Bull. Volcanol.* 75 (11). <http://dx.doi.org/10.1007/s00445-013-0762-x>.
- Edmonds, M., Herd, R.A., Galle, B., Oppenheimer, C.M., 2003. Automated, high time-resolution measurements of SO₂ flux at Soufrière Hills Volcano, Montserrat. *Bull. Volcanol.* 65 (8), 578–586.
- Eychenne, J., Pennec, J.-L., Troncoso, L., Gouhier, M., Nedelec, J.-M., 2012. Causes and consequences of bimodal grain-size distribution of tephra fall deposited during the August 2006 Tungurahua eruption (Ecuador). *Bull. Volcanol.* 74 (1), 187–205.
- Galle, B., Oppenheimer, C., Geyer, A., McConigle, A.J.S., Edmonds, M., Horrocks, L., 2003. A miniaturized ultraviolet spectrometer for remote sensing of SO₂ fluxes: a new tool for volcano surveillance. *J. Volcanol. Geotherm. Res.* 119 (1–4), 241–254.
- Galle, B., Johansson, M., Rivera, C., Zhang, Y., Kihlman, M., Kern, C., Lehmann, T., Platt, U., Arellano, S., Hidalgo, S., 2010. Network for Observation of Volcanic and Atmospheric Change (NOVAC) — a global network for volcanic gas monitoring: network layout and instrument description. *J. Geophys. Res. — Atmos.* 115 (D5), 2156–2202. <http://dx.doi.org/10.1029/2009JD011823>.
- Hall, M.L., Robin, C., Beate, B., Mothes, P., Monzier, M., 1999. Tungurahua Volcano, Ecuador: structure, eruptive history and hazards. *J. Volcanol. Geotherm. Res.* 91 (1), 1–21.
- Hall, M.L., Steele, A.L., Mothes, P.A., Ruiz, M.C., 2013. Pyroclastic density currents (PDC) of the 16–17 August 2006 eruptions of Tungurahua volcano, Ecuador: geophysical registry and characteristics. *J. Volcanol. Geotherm. Res.* 265, 78–93.
- Horwell, C., Baxter, P., 2006. The respiratory health hazards of volcanic ash: a review for volcanic risk mitigation. *Bull. Volcanol.* 69 (1), 1–24.
- Huppert, H., Woods, A., 2002. The role of volatiles in magma chamber dynamics. *Nature* 420, 493–495. <http://dx.doi.org/10.1038/nature01211>.
- Johansson, M., 2009. Application of Passive DOAS for Studies of Megacity Air Pollution and Volcanic Gas Emissions. (PhD Thesis), Chalmers University of Technology (64 pp.).
- Johansson, M., Galle, B., Rivera, C., Zhang, Y., 2009. Tomographic reconstruction of gas plumes using scanning DOAS. *Bull. Volcanol.* 71 (10), 1169–1178. <http://dx.doi.org/10.1007/s00445-009-0292-8>.
- Johnson, J.B., 2003. Generation and propagation of infrasonic airwaves from volcanic explosions. *J. Volcanol. Geotherm. Res.* 121, 1–14.
- Kern, C., Deutschmann, T., Vogel, L., Wöhrbach, M., Wagner, T., Platt, U., 2010. Radiative transfer corrections for accurate spectroscopic measurements of volcanic gas emissions. *Bull. Volcanol.* 72 (2), 233–247.
- Kumagai, H., Nakano, M., Maeda, T., Yepes, H., Palacios, P., Ruiz, M., Arrais, S., Vaca, M., Molina, I., Yamashima, T., 2010. Broadband seismic monitoring of active volcanoes using deterministic and stochastic approaches. *J. Geophys. Res. Solid Earth* 115 (B8), 2156–2202. <http://dx.doi.org/10.1029/2009JB006889>.
- Le Pennec, J.L., Jaya, D., Samaniego, P., Ramón, P., Moreno Yáñez, S., Egred, J., van der Plicht, J., 2008. The AD 1300–1700 eruptive periods at Tungurahua volcano, Ecuador, revealed by historical narratives, stratigraphy and radiocarbon dating. *J. Volcanol. Geotherm. Res.* 176 (1), 70–81.
- Le Pennec, J.-L., Ruiz, A., Ramón, P., Palacios, E., Mothes, P., Yepes, H., 2012. Impact of tephra falls on Andean communities: the influences of eruption size and weather conditions during the 1999–2001 activity of Tungurahua volcano, Ecuador. *J. Volcanol. Geotherm. Res.* 217–218, 91–103. <http://dx.doi.org/10.1016/j.jvolgeores.2011.06.011> (ISSN 0377-0273).
- Lyons, J.J., Waite, G.P., Rose, W.I., Chigna, G., 2010. Patterns in open vent, strombolian behavior at Fuego volcano, Guatemala, 2005–2007. *Bull. Volcanol.* 72, 1–15.
- Malinconico, L., 1979. Fluctuations in SO₂ emission during recent eruptions of Etna. *Nature* 278, 43–45.
- Mastin, L., Roeloffs, E., Beeler, N., Quick, J., 2008. Constraints on the size, overpressure, and volatile content of the Mount St. Helens magma system from geodetic and dome-growth measurements during the 2004–2006 + eruption: chapter 22. *A Volcano Rekindled: The Renewed Eruption of Mount St. Helens, 2004–2006*. USGS Professional Paper: 1750-22.
- McConigle, A.J.S., Oppenheimer, C., 2003. Optical sensing of volcanic gas and aerosol emissions. In: Oppenheimer, C., Pyle, D.M., Barclay, J. (Eds.), *Volcanic Degassing*. Geological Society, London. ISBN: 978-1-86239-136-9, pp. 149–168.
- Métrich, N., Bertagnini, A., Di Muro, A., 2010. Conditions of magma storage, degassing and ascent at Stromboli: new insights into the volcano plumbing system with inferences on the eruptive dynamics. *J. Petrol.* 51 (3), 603–626. <http://dx.doi.org/10.1093/petrology/egp083>.
- Millán, M., 1980. Remote sensing of air pollutants: a study of some atmospheric scattering effects. *Atmos. Environ.* 14, 1241–1253.
- Nakagawa, M., Wada, K., Thordarson, T., Wood, C.P., Gamble, J., 1999. Petrologic investigations of the 1995 and 1996 eruptions of Ruapehu volcano, New Zealand: formation of discrete and small magma pockets and their intermittent discharge. *Bull. Volcanol.* 61 (1–2). <http://dx.doi.org/10.1007/s004450050259>.
- Nicholson, E.J., Mather, T.A., Pyle, D.M., Odbert, H.M., Christopher, T., 2013. Cyclical patterns in volcanic degassing revealed by SO₂ flux time series analysis: an application to Soufrière Hills Volcano, Montserrat. *Earth Planet. Sci. Lett.* 375, 209–221.
- Ohba, T., Hirabayashi, J.-i., Nogami, K., Kusakabe, M., Yoshida, M., 2008. Magma degassing process during the eruption of Mt. Unzen, Japan in 1991 to 1995: modeling with the chemical composition of volcanic gas. *J. Volcanol. Geotherm. Res.* 175 (1–2), 120–132.
- Oppenheimer, C., 2003. Volcanic degassing. In: Rudnick, R.L. (Ed.), *The Crust. Treatise on Geochemistry*. Elsevier-Pergamon, Oxford, pp. 123–166.
- Platt, U., Stutz, J., 2008. Differential optical absorption spectroscopy. *Principles and Applications*. Springer, Berlin Heidelberg.
- Rouwet, D., Bellomo, S., Brusca, L., Inguaggiato, S., Jutzeler, M., Mora, R., Mazot, A., Bernard, R., Cassidy, M., Taran, Y., 2009. Major and trace element geochemistry of El Chichón volcano-hydrothermal system (Chiapas, Mexico) in 2006–2007: implications for future geochemical monitoring. *Geofis. Int.* 48 (1), 55–72.
- Salerno, G.G., Burton, M.R., Oppenheimer, C., Caltabiano, T., Randazzo, D., Bruno, N., Longo, V., 2009. Three-years of SO₂ flux measurements of Mt. Etna using an automated UV scanner array: comparison with conventional traverses and uncertainties in flux retrieval. *J. Volcanol. Geotherm. Res.* 183 (1–2), 76–83.
- Samaniego, P., Le Pennec, J.-L., Robin, C., Hidalgo, S., 2011. Petrological analysis of the pre-eruptive magmatic process prior to the 2006 explosive eruptions at Tungurahua volcano (Ecuador). *J. Volcanol. Geotherm. Res.* 199 (1–2), 69–84.
- Self, S., Gertisser, R., Thordarson, T., Rampino, M.R., Wolff, J.A., 2004. Magma volume, volatile emissions, and stratospheric aerosols from the 1815 eruption of Tambora. *Geophys. Res. Lett.* 31, L20608.
- Shinohara, H., 2008. Excess degassing from volcanoes and its role on eruptive and intrusive activity. *Rev. Geophys.* 46 (4), RG4005.
- Sparks, R.S.J., 2003. Dynamics of magma degassing. *Geol. Soc. Lond. Spec. Publ.* 213:5–22. <http://dx.doi.org/10.1144/GSL.SP.2003.213.01.02>.
- Sparks, R.S.J., Bursik, M.I., Carey, S.N., Gilbert, J.S., Glaze, L.S., Sigurdsson, H., Woods, A.W., 1997. *Volcanic Plumes*. John Wiley & Sons Ltd., Chichester, England (574 pp.).
- Spilliaert, N., Métrich, N., Allard, P., 2006. S–Cl–F degassing pattern of water-rich alkali basalt: modelling and relationship with eruption styles on Mount Etna volcano. *Earth Planet. Sci. Lett.* 248 (3–4), 772–786. <http://dx.doi.org/10.1016/j.epsl.2006.06.031> (ISSN 0012-821X).
- Steele, A., Ruiz, M., Anzieta, A., Johnson, J., 2014. Similarities in eruption dynamics: a seismo-acoustic analysis of explosion sequences at Tungurahua volcano in May–July 2010 & December 2012. Poster Presentation: European Geosciences Union (EGU) General Assembly; 2014 April 27–May 2; Vienna, Austria.
- Stoiber, R., Malinconico, L., Williams, S.N., 1983. Use of the correlation spectrometer at volcanoes. In: Tazieff, H., Sabroux, J.-C. (Eds.), *Forecasting Volcanic Events*. Elsevier, Amsterdam, pp. 425–444.
- Symonds, R.B., Rose, W.I., Bluth, G.J.S., Gerlach, T.M., 1994. Volcanic-gas studies: methods, results and applications. In: Carroll, M.R., Holloway, J.R. (Eds.), *Volatiles in Magmas*. Mineralogical Society of America, Washington, D.C., pp. 1–66.
- Vaselli, O., Tassi, F., Duarte, E., Fernandez, E., Poreda, R.J., Huertas, A.D., 2010. Evolution of fluid geochemistry at the Turrialba volcano (Costa Rica) from 1998 to 2008. *Bull. Volcanol.* 72 (4), 397–410.
- Wadge, G., 1981. The variation of magma discharge during basaltic eruptions. *J. Volcanol. Geotherm. Res.* 11 (2–4), 139–168. [http://dx.doi.org/10.1016/0377-0273\(81\)90020-2](http://dx.doi.org/10.1016/0377-0273(81)90020-2).
- Wright, H., Cashman, K., Mothes, P., Hall, M., Ruiz, A., Le Pennec, J.-L., 2012. Estimating rates of decompression from textures of erupted ash particles produced by 1999–2006 eruptions of Tungurahua volcano, Ecuador. *Geology* 40, 619–622. <http://dx.doi.org/10.1130/G32948.1>.
- Zhang, Y., Johansson, M., 2009. Mobile-DOAS Software. Optical Remote Sensing Group Chalmers University of Technology, Sweden (Copyright © 2004–2009).
- Zuccarello, L., Burton, M., Saccorotti, G., Bean, C., Patané, D., 2013. The coupling between very long period seismic events, volcanic tremor, and degassing rates at Mount Etna volcano. *J. Geophys. Res. Solid Earth* 118, 4910–4921. <http://dx.doi.org/10.1002/jgrb.5036>.